

# Variations of Flux Intensity in Large Features and Spectral Lines of $\alpha^2$ CVn in Ultraviolet \*

Sokolov N. A.

Central Astronomical Observatory at Pulkovo, St. Petersburg, Russia

**Abstract.** Variation of flux intensity at the cores of large features and spectral lines of the classical magnetic CP star  $\alpha^2$  CVn in the ultraviolet spectral region from 1150 to 3200 Å is investigated. This study is based on the archival *International Ultraviolet Explorer* data obtained at different phases of the rotational cycle. The shapes of two light curves at  $\lambda\lambda$  1375, and 1415 Å at the core of a large feature at  $\lambda$  1400 Å significantly differ. The light curve at  $\lambda$  1375 Å shows a similar shape as in the “pseudo-continuum”. The same behaviour of the flux is found at the cores of Si II resonance lines at  $\lambda\lambda$  1260–64 and 1485 Å, while the light curve at  $\lambda$  1415 Å shows the phase displacement of the flux minimum. The phase displacement is also present at the cores of the Si II resonance lines at  $\lambda\lambda$  1304–09 and 1485 Å. Minimal values of the amplitude of flux variations are reached at the cores of large features at  $\lambda\lambda$  1560 and 1770 Å and at the cores of strong Si II resonance lines. The flux at the cores of a large feature at  $\lambda$  1770 Å and Fe II resonance line at  $\lambda$  1725–31 Å does not vary within measurement errors. The investigation of the flux variability in the wings of Ly $_{\alpha}$  line indicates that the fluxes, which formed in the inner layers of the atmosphere are redistributed into the outer layers of the atmosphere of  $\alpha^2$  CVn.

**Key words:** stars: chemically peculiar – stars: individual:  $\alpha^2$  CVn – stars: variables: other

## 1 Introduction

The magnetic Chemically Peculiar (mCP) star  $\alpha^2$  CVn (HD 112413, HR 4915) displays strong line profile variations in the visual spectral region, attributable to the non-uniform chemical abundance distribution on the stellar surface, particularly of the lines of Fe, Cr and Ti (Khokhlova & Pavlova, 1984), Eu, Cr and Si (Goncharskii et al., 1983) and O (Gonzalez & Artru, 1994). Ryabchikova et al. (1999) report the first identification of the Eu III  $\lambda$  6666.347 line in the spectrum of  $\alpha^2$  CVn. Later Kochukhov et al. (2002) used a new magnetic Doppler Imaging code to reconstruct the magnetic field geometry and surface abundance distributions for six chemical elements of this star.

The study in the ultraviolet has been restricted to a much lower resolution, usually without resolving the individual stellar lines (e.g., Leckrone & Snijders, 1979). Hensberge et al. (1986) identified the ions Mg II, Si II, Cr II, Mn II, Fe II, Fe III, Co II, Ni II, Yb II and W II in the mid-ultraviolet spectrum of  $\alpha^2$  CVn, which has been obtained with the BUSS (Balloon-Borne Ultraviolet Spectrograph). High-dispersion IUE observations of the two resonance lines of Mg II, at  $\lambda\lambda$  1650

---

\* Based on INES data from the *IUE* satellite

and 1942 Å, were investigated by Leckrone (1984) for two normal stars, six HgMn stars and for the magnetic variable  $\alpha^2$  CVn. The last star possesses moderately strong Hg II resonance lines, confirming its classification as Hg-rich, but its magnesium anomaly is less pronounced than that of the MgMn stars. Fuhrmann (1989) investigated the high-resolution spectra of the CP star HR 465. For comparison purposes, the spectra of some other stars, including  $\alpha^2$  CVn, were discussed as well. The author have noted that the C II resonance doublet at  $\lambda$  1334.5–1335.7 Å is comparatively weak in the spectrum of  $\alpha^2$  CVn.

To quantify the ultraviolet variations of the CIV doublet at  $\lambda\lambda$  1548, 1550 Å, Shore et al. (1987) have formed the photometric line index, expressed in magnitudes. Later, Sokolov (2000, 2006) has introduced analogous photometric indices in order to derive the variations of the total absorption in the broad features at the far-UV spectral region. Unfortunately, these indices depend strongly upon the intensity stability of the near continuum. Based on the fact that the *IUE* Newly Extracted Spectra (INES) data are presented in absolute units, it is possible to investigate the flux variations at the cores of the large features and spectral lines. Recently, such an attempt has been made by Sokolov (2010) for an mCP star 56 Ari. Another mCP star for which there are enough *IUE* data in order to investigate the flux variability at the cores of the large features and spectral lines is  $\alpha^2$  CVn. This is done in the present paper.

## 2 Observational Data and Analysis

### 2.1 *IUE* Spectra

The *IUE* spectra used in this study are low-resolution echelle spectra obtained with a resolution of about 6 Å. Additionally, the “rebinned” spectra from high-dispersion images of  $\alpha^2$  CVn were used as well. In all cases, the spectra were obtained through a large aperture ( $9.5'' \times 22''$ ). Finally, we analyzed 22 SWP, 10 LWR and 6 LWP spectra, distributed quite smoothly over the period of rotation. The description of these *IUE* spectra in detail is done by Sokolov (2011).

### 2.2 Data Analysis

To analyse the *IUE* spectra of  $\alpha^2$  CVn we used the linearized least-squares method. An attempt was made to describe the light curves in a quantitative way by adjusting a Fourier series. The method was already applied to the *IUE* data of  $\alpha^2$  CVn and has shown very good descriptions of the monochromatic light curves in the “pseudo-continuum” (Sokolov, 2011). Thus, the observations were also fitted by a simple cosine wave:

$$F(\lambda, T') = A_0(\lambda) + A_1(\lambda) \cos(\omega T' + \phi_i(\lambda)), \quad (1)$$

where  $F(\lambda, T')$  is a flux for the given  $\lambda$ ,  $T' = T - T_0$  and  $\omega = 2\pi/P$ . The  $T_0$  and  $P$  are zero epoch and rotational period of the Farnsworth (1932) ephemeris, respectively. The coefficients  $A_0(\lambda)$  of the fitted curves define the average distribution of energy over the cycle of variability, while the coefficients  $A_1(\lambda)$  define the semi-amplitude of the flux variations for the given  $\lambda$ .

## 3 Identification of Large Features and Spectral Lines in the Spectrum of $\alpha^2$ CVn

In the far-UV spectral region silicon appears as the main absorber with the strong resonance lines at  $\lambda\lambda$  1260–64, 1304–09, 1485, 1526–33 Å (see Fig. 2 of Sokolov, 2011). It should be noted that the blend at  $\lambda$  1304–09 Å has two major contributors: the resonance doublet and the auto ionising multiplets (Artru & Lanz, 1987). According to Artru & Lanz (1987), strong lines in the spectrum of

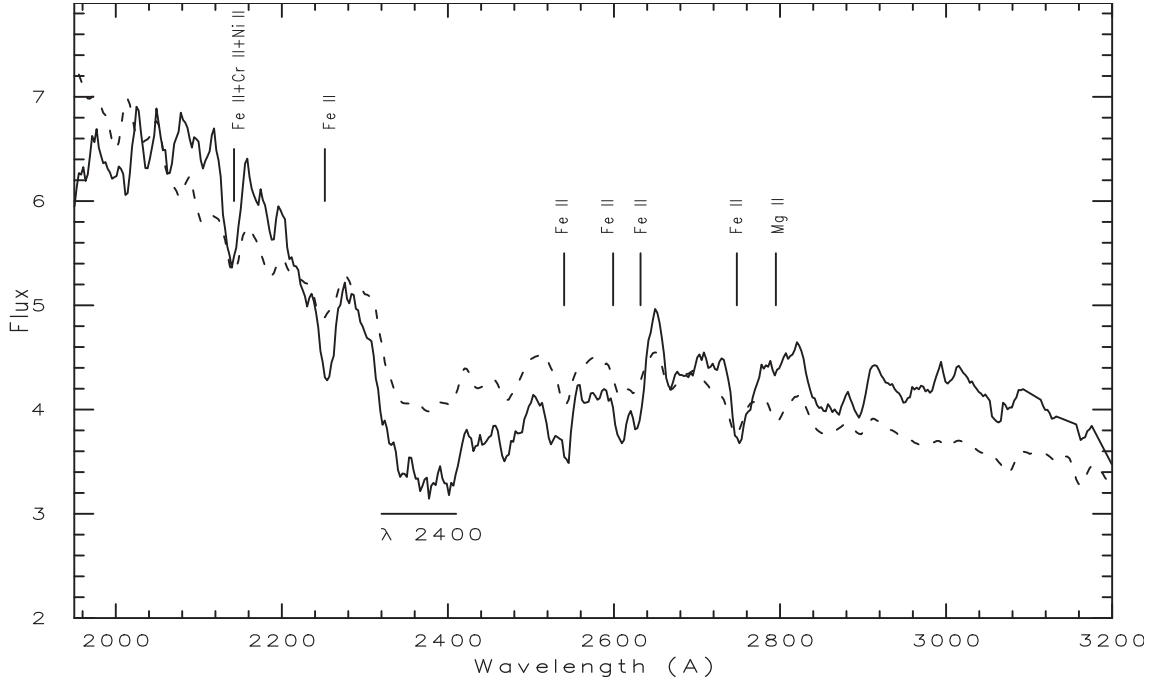


Figure 1: Average distributions of energy in  $10^{-10} \text{ ergs}^{-1} \text{ cm}^{-2} \text{ \AA}^{-1}$  of  $\alpha^2 \text{ CVn}$  (the solid line) and 56 Ari (the dashed line). The prominent spectral lines and features are shown by vertical and horizontal lines, respectively (see text).

CP stars appear from C II at  $\lambda 1334 \text{ \AA}$  and Al II at  $\lambda 1671 \text{ \AA}$ , which is close to a strong C I at  $\lambda 1657 \text{ \AA}$  line. Fe II form a depression at  $\lambda 1725-31 \text{ \AA}$  and Cr II produces a line at  $\lambda 1434 \text{ \AA}$ . Although in the case of  $\alpha^2 \text{ CVn}$  the line from C II at  $\lambda 1334 \text{ \AA}$  is not detectable at this resolution. Moreover, the C II resonance doublet at  $\lambda 1334.5-1335.7 \text{ \AA}$  is comparatively weak at the high-resolution spectrum of this star (Fuhrmann, 1989).

In the previous study of the star 56 Ari we identified which elements are responsible for the depressions of flux centred at  $\lambda\lambda 2140, 2250, 2540, 2607, 2624$  and  $2747 \text{ \AA}$  (Sokolov, 2010). The synthetic spectrum calculation showed that Fe II appears as the main absorber for these depressions. On the other hand, the same synthetic spectrum calculation showed that mainly Fe, Cr and Ni are responsible for the flux depression at  $\lambda 2140 \text{ \AA}$ . A comparison of the average energy distribution of  $\alpha^2 \text{ CVn}$  with the average energy distribution of 56 Ari showed that the depressions of the flux centred at  $\lambda\lambda 2140, 2250, 2540, 2607, 2624$  and  $2747 \text{ \AA}$  are also present in the spectrum of  $\alpha^2 \text{ CVn}$ . It is well known that the Mg II resonance lines at  $\lambda\lambda 2795, 2798$  and  $2803 \text{ \AA}$  are responsible for the depression of the flux at  $\lambda 2800 \text{ \AA}$ . This depression is not detectable in the low-resolution mode in the spectrum of  $\alpha^2 \text{ CVn}$ . Prominent depressions of the flux in the near-UV spectral region are indicated in Fig. 1 with their identifications. In order to compare the mean energy distributions of  $\alpha^2 \text{ CVn}$  and 56 Ari, the fluxes of 56 Ari were increased by the factor of ten in Fig. 1.

Four large features at  $\lambda\lambda 1400, 1560, 1770$  and  $2350-2400 \text{ \AA}$ , which are strongly enhanced in the spectrum of CP stars, are well seen in spectrum of  $\alpha^2 \text{ CVn}$ . Lanz et al. (1996) have given strong arguments supporting the idea that the intense autoionisation resonances of Si II could explain the features at  $\lambda 1400$  and  $1560 \text{ \AA}$  in the spectrum of CP stars. On the other hand, they were unable to identify the depression of the flux at  $\lambda 1770 \text{ \AA}$ . Another element may cause this strong depression. A comparison of the *IUE* high resolution spectrum of 56 Ari with the full synthetic spectrum, as well as those, including the lines from only one element has shown that metal is responsible for the depression of the flux at  $\lambda 1770 \text{ \AA}$  (see Fig. 9 of Sokolov, 2006). It is necessary to note that

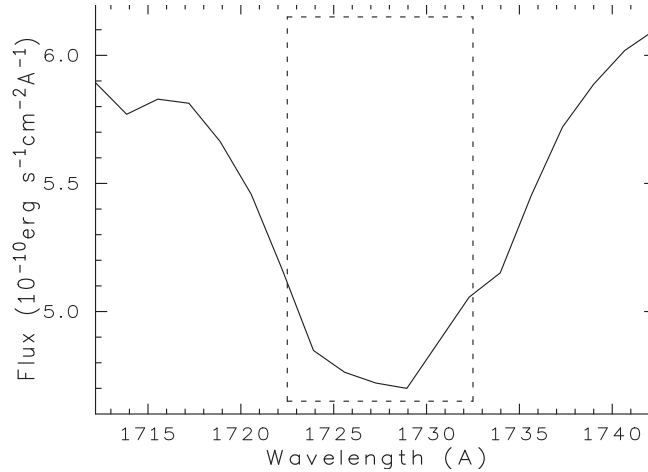


Figure 2: The spectral region of Fe II doublet at  $\lambda 1725-31 \text{ \AA}$  of  $\alpha^2 \text{ CVn}$ . The rectangle shows the selected spectral region for the calculation of the average intensity at the core of this doublet.

this depression is considerably increased in the spectrum of  $\alpha^2 \text{ CVn}$  than that in the spectrum of 56 Ari. The large features at  $\lambda 2350-2400 \text{ \AA}$ , which are strongly enhanced in the spectrum of CP stars, are well seen in the spectrum of  $\alpha^2 \text{ CVn}$ . The lines of the metal peak elements have a particularly important contribution to the opacity at  $\lambda 2350-2400 \text{ \AA}$ . Adelman et al. (1993) have given strong arguments supporting the idea that a large number of metal lines can explain the feature at  $\lambda 2350-2400 \text{ \AA}$ . Many CP stars have here a very pronounced flux depression compared to normal stars (Stepień & Czechowski, 1993).

#### 4 Average Flux Determination at the Cores of Large Features and Spectral Lines in the Spectrum of $\alpha^2 \text{ CVn}$

To measure the absorption at the cores of large features, the spectra were processed using the spectral reduction software SPE developed by S. Sergeev at the Crimean Astrophysical Observatory (CrAO). The program allows measuring the average flux intensity and the corresponding error in any selected rectangular spectral region. For the large features at  $\lambda 1560$  and  $1770 \text{ \AA}$  the spectral regions are  $\sim 10 \text{ \AA}$  wide, while for the largest feature at  $\lambda 1400 \text{ \AA}$  two spectral regions were selected and centred at  $\lambda 1375$  and  $1415 \text{ \AA}$ . On the other hand, for the large feature at  $\lambda 2350-2400 \text{ \AA}$  the spectral region was used with  $\sim 50 \text{ \AA}$  wide and centred at  $\lambda 2375 \text{ \AA}$ .

The resonance doublets of Si II and Fe II lines are seen as depressions in the *IUE* low-resolution spectrum of  $\alpha^2 \text{ CVn}$ , as illustrated by Fig. 2. Thus, the average intensity of the flux at the cores of the spectral lines was computed by averaging five nearest fluxes for a given  $\lambda$ :

$$F(\lambda) = \frac{1}{5} \sum_{i=1}^5 F(\lambda - \lambda_{\text{step}} \cdot (i - 3)), \quad (2)$$

where  $\lambda_{\text{step}}$  is equal to  $1.676 \text{ \AA}$  and  $2.669 \text{ \AA}$  for a SWP camera, and for LWR and LWP cameras, respectively. As far as the errors in  $F(\lambda)$  are concerned, we computed them by taking into account the errors in the fluxes as presented in the *INES Catalog*, according to the standard error propagation theory. In order to check the reliability of the average flux intensity at the cores of spectral lines, the spectra were also processed using the SPE program. Experience shows that within the measurement errors the average flux intensity computed by the SPE program, and using equation (2) are the same.

#### 4.1 Variations of Large Features

Left part of Figure 3 exhibits variations of average intensity of the fluxes at the cores of large features versus the rotational phase. First of all, the shapes of two light curves at the core of a large feature at  $\lambda 1400 \text{ \AA}$  significantly differ. The minimum of the light curve at  $\lambda 1375 \text{ \AA}$  is reached at phase 0.05 while the minimum of the light curve at  $\lambda 1415 \text{ \AA}$  is at phase 0.26. However, the amplitudes of two light curves at  $\lambda 1375$  and  $1415 \text{ \AA}$  are approximately the same and are equal to 0.41 and  $0.32 \cdot 10^{-10} \text{ erg s}^{-1} \text{ cm}^{-2} \text{ \AA}^{-1}$ , respectively. According to the model computation of Lanz et al. (1996), two features at  $\lambda 1400$  and  $1560 \text{ \AA}$  are connected with the intense autoionisation resonance of Si II. A qualitative comparison of the light curves at  $\lambda 1375$  and  $1560 \text{ \AA}$  shows a good agreement. The minimum of the light curve at  $\lambda 1375 \text{ \AA}$  is reached at phase 0.05 while the minimum of the light curve at  $\lambda 1560 \text{ \AA}$  is at phase 0.10. Also, the amplitudes of two light curves at  $\lambda 1375$  and  $1560 \text{ \AA}$  are approximately the same and are equal to 0.41 and  $0.38 \cdot 10^{-10} \text{ erg s}^{-1} \text{ cm}^{-2} \text{ \AA}^{-1}$ , as illustrated by Fig. 3.

The identifications of two features at  $\lambda 1770$  and  $2375 \text{ \AA}$  are connected with a large concentration of metal lines (see Sect. 3). The flux variations at the cores of the features at  $\lambda 1770$  and  $2375 \text{ \AA}$  also significantly differ. Thus, the amplitude of the light curve at the core of the feature at  $\lambda 1770 \text{ \AA}$  is equal to  $0.11 \cdot 10^{-10} \text{ erg s}^{-1} \text{ cm}^{-2} \text{ \AA}^{-1}$ . Practically, the flux at the core of this feature does not vary within the measurement errors. On the other hand, the amplitude of the light curve at the core of the feature at  $\lambda 2375 \text{ \AA}$  is equal to  $0.43 \cdot 10^{-10} \text{ erg s}^{-1} \text{ cm}^{-2} \text{ \AA}^{-1}$ . However, the shapes of light curves are approximately the same, as illustrated by Fig. 3. One can see that the behavior of the flux is different at the cores of large features, even if the same element is responsible for the features. This puzzling situation was one of the incentives for studying the variations of the flux at the cores of the Si II resonance lines and the depressions for which a concentration of Fe II lines is responsible.

#### 4.2 Variations of Si II Resonance Lines

Even in normal stars Si II appears as the main absorber with the strongest resonance lines recognizable at  $\lambda 1260-64$ ,  $1304-09$ ,  $1485$ ,  $1526-33 \text{ \AA}$  (Artru & Lanz, 1987). Right part of Figure 3 exhibits the flux variations at the cores of these depressions versus the rotational phase. Note that the vertical scales are the same for each part of the figure. One can see from Fig. 3 that the light curves have similar shapes in the cores of resonance lines at  $\lambda 1260-64$  and  $1526-33 \text{ \AA}$ . The minima of the light curves at  $\lambda 1260-64$  and  $1526-33 \text{ \AA}$  are reached at phases 0.05 and 0.02, respectively. A similar behaviour is revealed by the nearest monochromatic light curves in the “pseudo-continuum” (see Fig. 3 of Sokolov, 2011). Also, the amplitudes of the light curves at the cores of depressions at  $\lambda 1260-64$  and  $1526-33 \text{ \AA}$  are in good agreement and are equal to 0.49 and  $0.63 \cdot 10^{-10} \text{ erg s}^{-1} \text{ cm}^{-2} \text{ \AA}^{-1}$ , respectively. It should be noted that the light curve at  $\lambda 1375 \text{ \AA}$  shows a similar shape. On the other hand, the minima of the light curves at  $\lambda 1304-09$  and  $1485 \text{ \AA}$  are reached at phases 0.12 and 0.30, as illustrated by Fig. 3. However, the minima of the monochromatic light curves are reached at phase  $\sim 0.0$  in the nearest “pseudo-continuum”. Moreover, the amplitudes of the light curves are different at  $\lambda 1304-09$  and  $1485 \text{ \AA}$  and amount to 0.38 and  $0.64 \cdot 10^{-10} \text{ erg s}^{-1} \text{ cm}^{-2} \text{ \AA}^{-1}$ , respectively. It should be noted that the light curve at  $\lambda 1415 \text{ \AA}$  reveals a similar shape. The monochromatic light curves in the near-UV spectral region with  $\lambda > 2505 \text{ \AA}$  in the “pseudo-continuum” also demonstrate such behaviour. The near-UV spectral region is quite important in order to investigate the variability of the flux at the cores of Fe II lines.

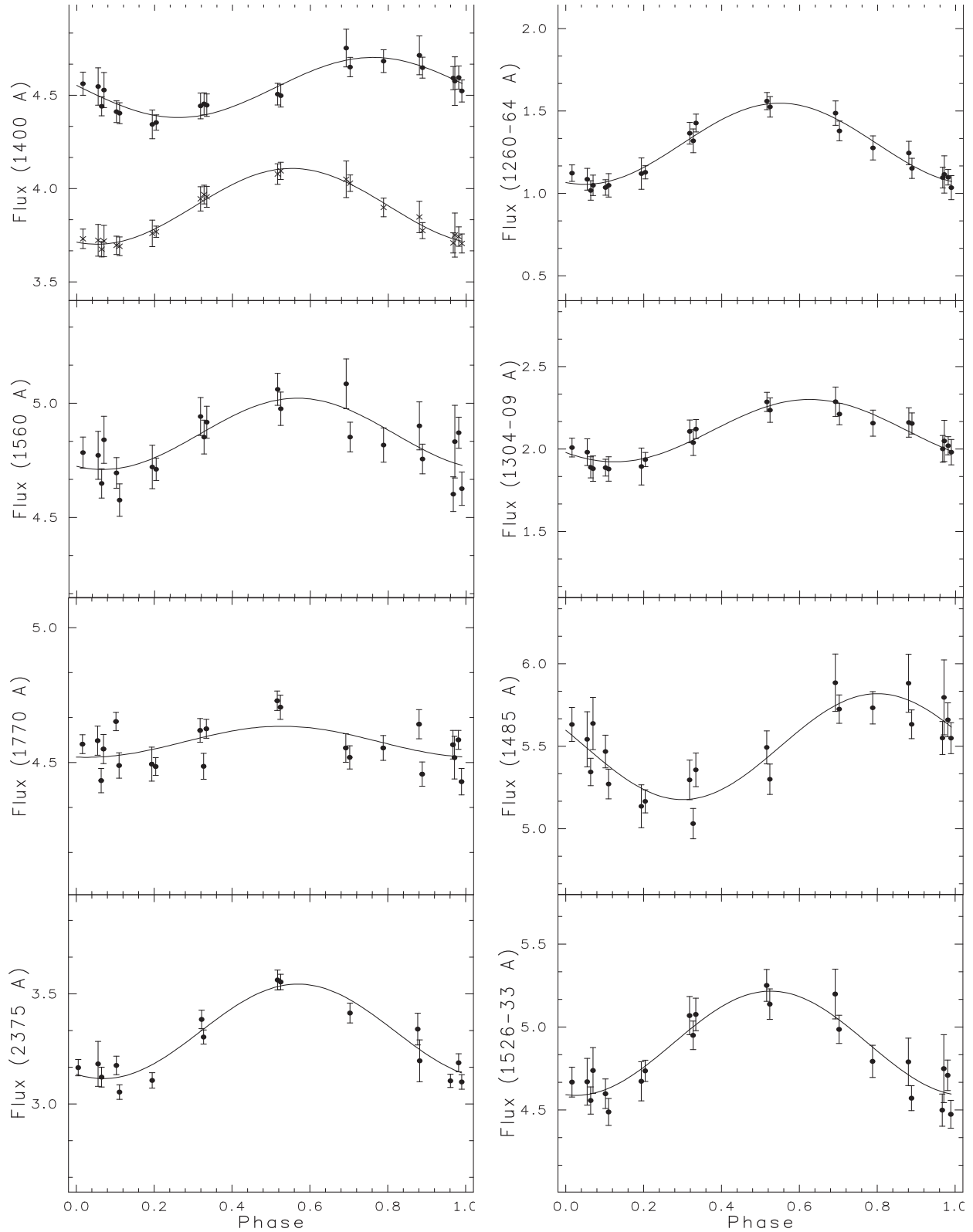


Figure 3: **Left:** Phase diagrams of the light curves in the cores of large features in  $10^{-10} \text{ erg s}^{-1} \text{ cm}^{-2} \text{ \AA}^{-1}$  for  $\alpha^2 \text{ CVn}$ . The upper panel represents two phase diagrams centred at  $\lambda 1375 \text{ \AA}$  (crosses) and at  $\lambda 1415 \text{ \AA}$  (circles).  $1\sigma$  error bars accompany each data point. Solid lines denote the fit according to equation (2). **Right:** Phase diagrams of the light curves at the cores of Si II resonance lines.

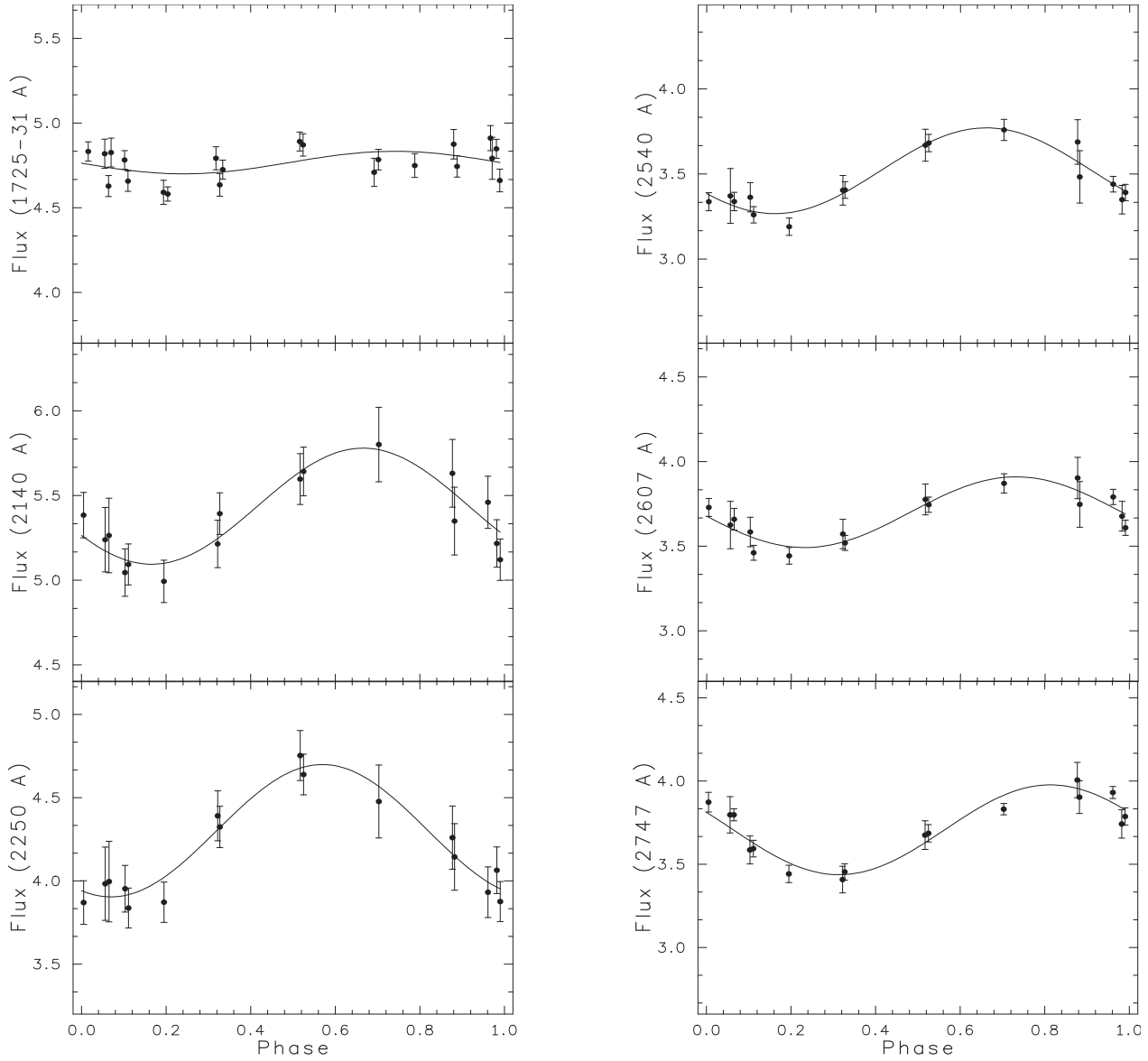


Figure 4: The same as in Fig. 3 for the light curves at the cores of Fe II lines

### 4.3 Variations of Fe II Lines

In the far-UV spectral region the Fe II doublet at  $\lambda 1725-31 \text{ \AA}$  gives only one depression of the flux (Artru & Lanz, 1987). A synthetic spectrum calculation shows that Fe II appears as the main absorber of the flux at  $\lambda \lambda 2250, 2540, 2607, 2624$  and  $2747 \text{ \AA}$  (see Sect. 3). Additionally, the flux depression at  $\lambda 2140 \text{ \AA}$  was included in our investigation. On the other hand, two depressions of the flux at  $\lambda \lambda 2607$  and  $2624 \text{ \AA}$  have shown the same behaviour. Thus, we have included in our investigation only the flux depression at  $\lambda 2607 \text{ \AA}$ . Figure 4 exhibits the variations of average intensity of the flux at the cores of Fe II lines versus the rotational phase. Note that the vertical scales are the same for each part of the figure. As we can see on the graphs of Fig. 4, the variability of the flux at the cores of Fe II lines reveals approximately the same behaviour as the monochromatic light curves with  $\lambda > 2505 \text{ \AA}$  in the “pseudo-continuum” (see. Fig. 3 of Sokolov, 2011). The light curves at the cores of Fe II lines show a phase displacement of the flux minimum from 0.07 at  $\lambda 2250 \text{ \AA}$  to 0.31 at  $\lambda 2747 \text{ \AA}$ . Additionally, the minimum of the light curve at the core of Fe II lines at  $\lambda 2140 \text{ \AA}$  is located

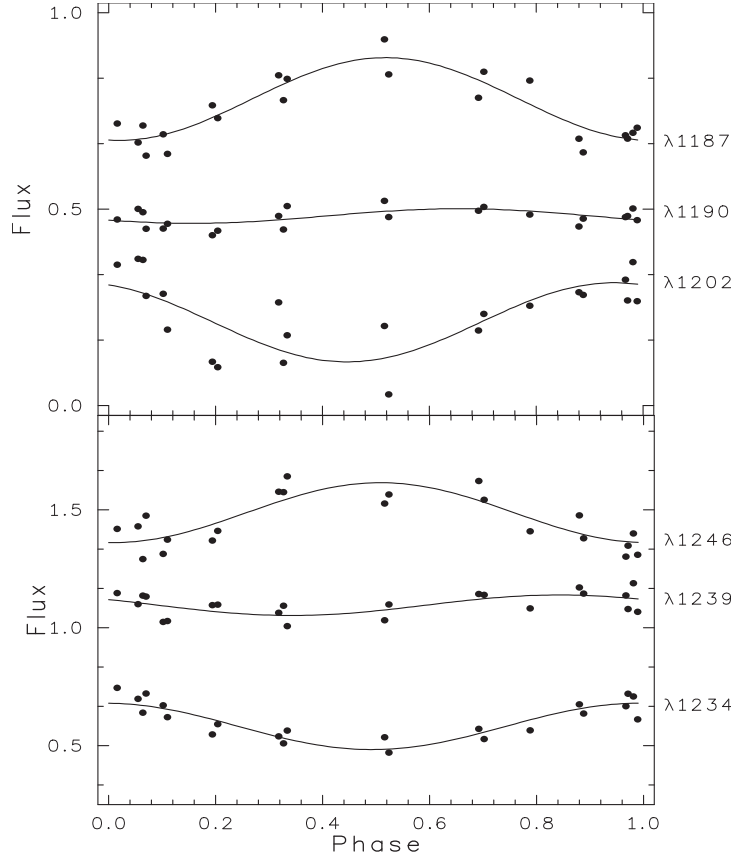


Figure 5: Phase diagrams of the light curves in  $10^{-10} \text{ erg s}^{-1} \text{ cm}^{-2} \text{ \AA}^{-1}$  in the wings of  $\text{Ly}_\alpha$  line for  $\alpha^2 \text{ CVn}$ . Upper and lower panels show short-wavelength and long-wavelength sides of the  $\text{Ly}_\alpha$  line, respectively. Solid lines denote the fit according to equation (2).

at phase 0.16. However, the amplitude of the light curve at  $\lambda 2140 \text{ \AA}$  is large enough and is equal to  $0.69 \cdot 10^{-10} \text{ erg s}^{-1} \text{ cm}^{-2} \text{ \AA}^{-1}$ . It is due possibly to the fact that mainly three chemical elements (Fe, Cr, Ni) are responsible for this depression. The monochromatic light curves in the “pseudo-continuum” only with  $\lambda > 2505 \text{ \AA}$  demonstrate the same phase displacement of the flux minimum. It should be noted that the amplitudes of the light curves here are larger than those at the cores of Fe II lines. On the other hand, we have the light curve at the core of Fe II resonance line at  $\lambda 1725 - 31 \text{ \AA}$ , where the amplitude is equal to  $0.13 \cdot 10^{-10} \text{ erg s}^{-1} \text{ cm}^{-2} \text{ \AA}^{-1}$ . Similar to the situation at the core of a large feature at  $\lambda 1770 \text{ \AA}$  the flux does not vary at the core of this line either. However, the variability of the flux in the nearest “pseudo-continuum” is significant. Thus, the amplitudes of the monochromatic light curves at  $\lambda \lambda 1690$  and  $1794 \text{ \AA}$  are equal  $0.41$  and  $0.51 \cdot 10^{-10} \text{ erg s}^{-1} \text{ cm}^{-2} \text{ \AA}^{-1}$ , respectively.

#### 4.4 Variations of Lyman-Alpha Line

Leckrone & Snijders (1979) have compared the Lyman-alpha ( $\text{Ly}_\alpha$ ) profiles of  $\alpha^2 \text{ CVn}$  at two phases, 0.0 and 0.5, using the *Copernicus* data. The authors have drawn the conclusion that brightness variations at the core of  $\text{Ly}_\alpha$  line are anomalous with respect to the adjacent ultraviolet regions. In addition, they noted that the coverage of the complete cycle by a future space instrument will be necessary to establish the specific phasing of these variations. Based on the fact that the star is bright enough ( $m_v = 2.90$ ), the *IUE* data have allowed to investigate the behavior of the monochromatic light curves in the short-wavelength and long-wavelength sides from the core of the  $\text{Ly}_\alpha$  line.

Several monochromatic light curves in the wings of the Ly $_{\alpha}$  line at different wavelengths were formed. Figure 5 exhibits the flux variations in the short-wavelength and long-wavelength sides of the Ly $_{\alpha}$  line versus the rotational phase. As we can see on the graphs of Fig. 5, the monochromatic light curves have identical shapes in the short-wavelength and long-wavelength sides of the Ly $_{\alpha}$  line. The light curves at  $\lambda\lambda$  1187 and 1246 Å show the minimum and maximum of the flux at phases 0.0 and 0.5, respectively. Note that the monochromatic light curves in the “pseudo-continuum” show the same behaviour in the far-UV spectral region. These monochromatic light curves are most removed from the line centre of Ly $_{\alpha}$  at  $\lambda$  1215 Å. On the other hand, the monochromatic light curves at  $\lambda\lambda$  1202 and 1234 Å reveal the flux minimum and maximum at phases 0.5 and 0.0, respectively. Also, the light curve in the V filter shows the same behaviour in the visual spectral region (Pyper, 1969). At the same time, the variation of the flux at  $\lambda\lambda$  1190 and 1239 Å is practically zero over the period of rotation. In other words, the so-called “null wavelength regions” are also disposed in these wavelengths. It should be noted that the fluxes at the cores of the Ly $_{\alpha}$  line varies with small amplitudes at  $\lambda$  1213 Å for two CP stars CU Vir and 56 Ari (Sokolov, 2000, 2006).

## 5 Discussion

Our results indicate that the variations of the average flux intensity at the cores of large features and spectral lines show different behaviours. First of all, the shapes of two light curves at  $\lambda\lambda$  1375 and 1415 Å at the core of a large feature at  $\lambda$  1400 Å curves significantly differ. The minimum of the light curve at  $\lambda$  1375 Å is reached at phase 0.05, while the minimum of the light curve at  $\lambda$  1415 Å is located at phase 0.26. However, the difference in wavelength between these spectral regions amounts to 40 Å. This puzzling situation was one of the incentives for studying the high-dispersion spectra of  $\alpha^2$  CVn in these spectral regions. In the top panel of Fig. 6 two high-dispersion spectra are plotted in the spectral region near  $\lambda$  1375 Å. These spectra SWP 27894 and SWP 15828 were obtained at phases 0.064 (the dashed line) and 0.524 (the solid line), respectively. From Fig. 6 we see that the fluxes of the spectrum SWP 27894 are systematically lower than the fluxes of the spectrum SWP 15828. In the bottom panel of Fig. 6 two high-dispersion spectra are plotted in the spectral region near  $\lambda$  1415 Å. These spectra SWP 04813 and SWP 27880 were obtained at the phases 0.204 (dashed line) and 0.702 (full line), respectively. Again, we can see that the fluxes of the spectrum SWP 04813 are lower than the fluxes of the spectrum SWP 27880. The comparisons of the high-dispersion spectra in the spectral regions of the broad feature at  $\lambda$  1400 Å are in agreement with the phase diagrams obtained from the low-dispersion spectra (see Fig. 3). However, the nature of this behaviour of the fluxes in the spectral regions at  $\lambda\lambda$  1375 and 1415 Å is still unclear. Possibly, the effect of different species of spectral lines can play some role here.

The light curves at the cores of Si II resonance lines at  $\lambda\lambda$  1260–64 and 1526–33 Å show shapes, similar to the ones revealed in the “pseudo-continuum”. At the same time, the light curves at the cores of Si II resonance lines at  $\lambda\lambda$  1304–09 and 1485 Å demonstrate the phase displacement of the flux minimum. On the other hand, the flux at the cores of a large feature at  $\lambda$  1770 Å and Fe II resonance line at  $\lambda$  1725–31 Å does not vary within the measurement errors. Moreover, the light curves at the cores of Fe II lines show the phase displacement of the flux minimum from 0.07 at  $\lambda$  2250 Å to 0.31 at  $\lambda$  2747 Å.

The vertically dependent abundance stratification in CP stars is suggested by many authors (e. g., Ryabchikova, 2008, and references therein). This effect may influence our results because the effective depth at which the fluxes are formed at  $\lambda < 2000$  Å can differ from the effective depth at which the fluxes are formed at  $\lambda > 2505$  Å. We can expect that the flux comes from the upper layers of the atmosphere at the cores of some large features and depressions than the flux coming from the nearest “pseudo-continuum” in the spectral region with  $\lambda < 2000$  Å. Therefore, possibly, some large features and depressions show the displacement of position of the flux minimum, though the flux

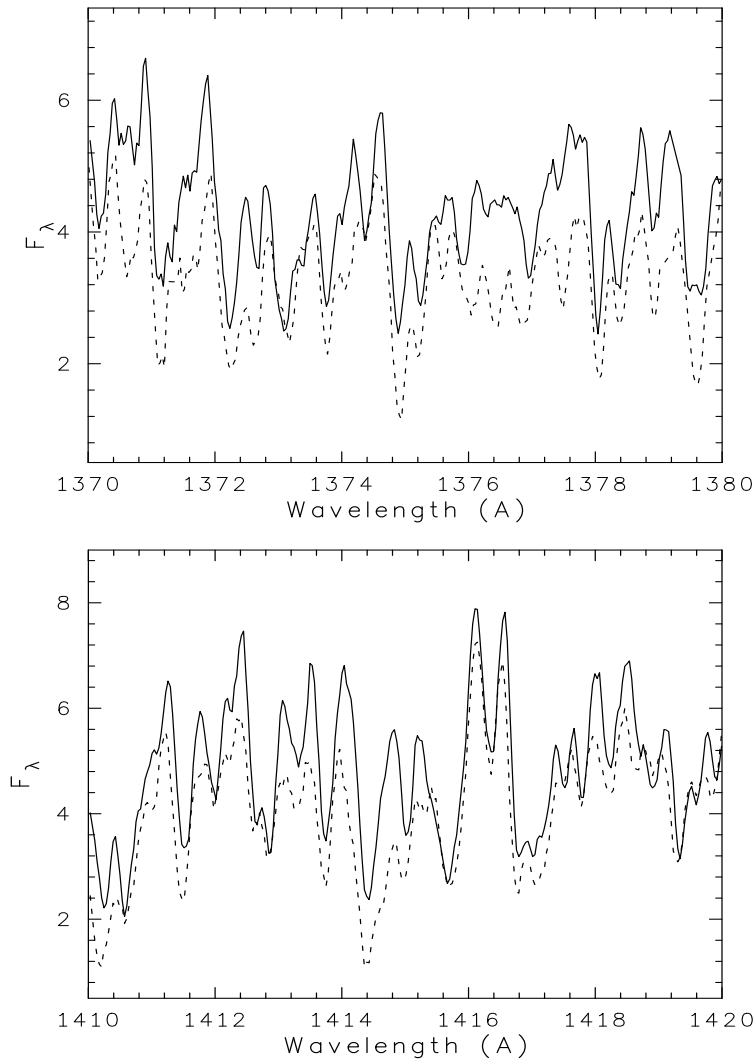


Figure 6: Two spectral regions of the broad feature at  $\lambda 1400 \text{ \AA}$  for  $\alpha^2 \text{ CVn}$ . The high-dispersion spectra in the region of  $\lambda 1375 \text{ \AA}$  (top panel) and the high-dispersion spectra in the region of  $\lambda 1415 \text{ \AA}$  (bottom panel) (see the text).

in the nearest “pseudo-continuum” does not reveal such a displacement. However, the spectrum in the “pseudo-continuum” is also blocked by a great number of spectral lines of various chemical elements.

The main thing is that the energy blocking by the silicon bound-free transitions and metal bound-bound transitions decreases the flux in the UV spectral region. The blocked flux appears in the visual and red parts of the spectrum. Such an explanation is supported by the anti-phase relationship of light curves in the visual and UV spectral regions. Probably, our investigation indicates that not only this mechanism may influence on the redistribution of the flux in atmosphere of  $\alpha^2 \text{ CVn}$ . The fluxes, situated in the wings of the  $\text{Ly}_\alpha$  line at different distances from its center are hence formed at different depths in the stellar atmosphere. The investigation of the flux variability in the wings of  $\text{Ly}_\alpha$  line indicates that the fluxes, which formed in the inner layers of atmosphere are redistributed into the outer layers of the atmosphere of  $\alpha^2 \text{ CVn}$ . Therefore, there should be a layer in the atmosphere of the star where the fluxes do not vary over the period of rotation. However, an independent investigation of the  $\text{Ly}_\alpha$  line variations in others CP stars is needed in order to confirm our results.

## 6 Conclusions

The archival *IUE* spectrophotometric data of  $\alpha^2$  CVn have permitted to analyse the light variations at the cores of large features and spectral lines. The variations of flux intensity at the cores of large features and spectral lines reveal various behaviours. The effect of different species of spectral lines is observed in different regions at  $\lambda\lambda$  1375 and 1415 Å of the large feature  $\lambda$  1400 Å. The light curve at  $\lambda$  1375 Å shows a similar shape like in the “pseudo-continuum”. The same behaviour of the flux is observed at the cores of Si II resonance lines at  $\lambda\lambda$  1260–64 and 1485 Å, while the light curve at  $\lambda$  1415 Å shows the phase displacement of the flux minimum. The phase displacement is also present at the cores of Si II resonance lines at  $\lambda\lambda$  1304–09 and 1485 Å. The same phase displacement is at the cores of the Fe II depressions in the spectral region with  $\lambda > 2505$  Å. However, the variability of the flux at the cores of the Fe II depressions in this spectral region is the same as in the “pseudo-continuum”.

The minimal values of the amplitude of the flux variations are reached at the cores of large features at  $\lambda\lambda$  1560 and 1770 Å and at the cores of the strong Si II resonance lines at  $\lambda\lambda$  1260–64, 1304–09 and 1485 Å. The flux at the cores of a large feature at  $\lambda$  1770 Å and Fe II resonance line at  $\lambda$  1725–31 Å does not vary within the measurement errors.

The investigation of the flux variability in the wings of the Ly $_{\alpha}$  line indicate that the fluxes, which formed in the inner layers of atmosphere are redistributed into the outer layers of the atmosphere of  $\alpha^2$  CVn. However, an independent investigation of the Ly $_{\alpha}$  line variations in the high-resolution mode is needed in order to confirm our results.

## References

- Adelman S. J., Cowley C. R., Leckrone D. S., Roby S. W., Wahlgren G. M., 1993, *ApJ*, 419, 276  
 Artru M.-C., Lanz T., 1987, *A&A*, 182, 273  
 Farnsworth G., 1932, *ApJ*, 75, 364  
 Fuhrmann K., 1989, *A&AS*, 80, 399  
 Goncharskii A. V., Ryabchikova T. A., Stepanov V. V., Khokholova V. L., Yagola A. G., 1983, *Soviet Astr.*, 14, 652  
 Gonzalez J. F., Artru M.-C., 1994, *A&A*, 289, 209  
 Hensberge H., Van Santvoort J., Van der Hucht K. A., Morgan T. H., 1986, *A&A*, 158, 113  
 Khokhlova V. L., Pavlova V. M., 1984, *Soviet Astr. Lett.*, 10, 158  
 Kochukhov O., Piskunov N., Ilyin I., Tuominen I., 2002, *A&A*, 389, 420  
 Lanz T., Artru M.-C., Le Dourneuf M., Hubeny T., 1996, *A&A*, 309, 218  
 Leckrone D. S., 1984, *ApJ*, 286, 725  
 Leckrone D. S., Snijders M. A. J., 1979, *ApJS*, 39, 549  
 Pyper D. M., 1969, *ApJS*, 18, 347  
 Ryabchikova T., 2008, *Contr. of the Astron. Obs. Skalnaté Pleso*, 38, 257  
 Ryabchikova T., Piskunov N., Savanov I., Kupka F., Malanushenko V., 1999, *A&A*, 343, 229  
 Shore S. N., Brown D. N., Sonneborn G., 1987, *AJ*, 94, 737  
 Sokolov N. A., 2000, *A&A*, 353, 707  
 Sokolov N. A., 2006, *MNRAS*, 373, 666  
 Sokolov N. A., 2010, *Astrophys. Space Sci.*, 330, 37  
 Sokolov N. A., 2011, this proceedings  
 Stepień K., Czechowski W., 1993, *A&A*, 268, 187